Article

Regioselective On-Surface Synthesis of [3]Triangulene Graphene Nanoribbons

Michael C. Daugherty, Peter H. Jacobse, Jingwei Jiang, Joaquim Jornet-Somoza, Reis Dorit, Ziyi Wang, Jiaming Lu, Ryan McCurdy, Weichen Tang, Angel Rubio,* Steven G. Louie,* Michael F. Crommie,* and Felix R. Fischer*

Read Online

ACCESS | Metrics & More | Article Recommendations | Supporting Information

ABSTRACT: The integration of low-energy states into bottom-up engineered graphene nanoribbons (GNRs) is a robust strategy for realizing materials with tailored electronic band structure for nanoelectronics. Low-energy zero-modes (ZMs) can be introduced into nanographenes (NGs) by creating an imbalance between the two sublattices of graphene. This phenomenon is exemplified by the family of [n]triangulenes ($n \in \mathbb{N}$). Here, we demonstrate the synthesis of [3]triangulene-GNRs, a regioregular one-dimensional (1D) chain of [3]triangulenes linked by five-membered rings. Hybridization between ZMs on adjacent [3]triangulenes leads to the emergence of a narrow band gap, $E_{g,exp} \sim 0.7$ eV, and topological end states that are experimentally verified using scanning tunneling spectroscopy. Tight-binding and first-principles density functional theory calculations within the local density approximation corroborate our experimental observations. Our synthetic design takes advantage of a selective on-surface head-to-tail coupling of monomer building blocks enabling the regioselective synthesis of [3]triangulene-GNRs. Detailed ab initio theory provides insights into the mechanism of on-surface radical polymerization, revealing the pivotal role of Au−C bond formation/breakage in driving selectivity.

On-Surface Synthesis of [3]Triangulene GNR

regioselective head-to-tail polymerization
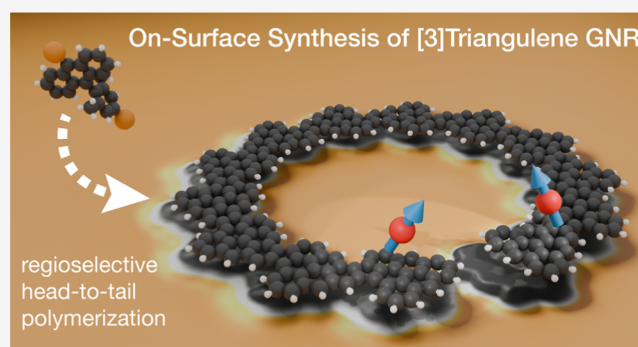
INTRODUCTION

Graphene nanoribbons (GNRs) are an emerging class of bottom-up synthesized carbon nanomaterials whose electronic structure can be tailored by the deterministic design of molecular precursors. Laterally confining graphene to a nanoribbon (width <2 nm) opens a highly tunable band gap that renders these materials attractive candidates for logic devices at the molecular scale.[1,2] More recently, the engineering of low-energy states in GNRs has emerged as a robust strategy to induce magnetic ordering in low-dimensional phases, superlattices of topologically protected junction states, and even intrinsically metallic band structures in bottom-up synthesized GNRs.[3−7] These advances have been realized by designing structures that imbue nanographenes (NGs) with a sublattice imbalance that gives rise to low-energy states.[8] A sublattice imbalance $\Delta N = N_A - N_B$, where N_A and N_B are the number of carbon atoms on the A and B sublattices, respectively, leads to ΔN eigenstates at $E = 0$ eV, or zero-modes (ZMs), that are polarized to the majority sublattice.[9] In a chemical picture, these ZMs can be described as the π-radicals associated with open-shell non-Kekuléan structures.[10] The interaction between adjacent ZMs can lead to hybridization and spin correlation effects shaping electronic structure and leading to the emergence of magnetism.[8] Triangular-

shaped [n]triangulenes are the archetype of sublattice imbalance in NGs and feature a ground-state spin that scales linearly with their size.[11−15] [3]triangulene features an $S = 1$ ground state and interactions between proximal ZMs on neighboring [3]triangulenes linked at their vertices have been studied in dimers,[16] trimers,[17] and one-dimensional (1D) spin chains.[18] Interactions between ZMs of triangulenes joined vertex-to-edge (thus connecting the majority and minority sublattices) remain unexplored.

Surface-catalyzed Ullmann-type coupling is a powerful technique for the bottom-up synthesis of [3]triangulene chains and GNRs.[19] The metal surface catalyzes the homolytic cleavage of weak carbon−halogen bonds, facilitating radical step-growth polymerization and subsequent cyclodehydrogenation to form a fully fused aromatic structure. Means of achieving chemoselectivity, however, are limited by the available on-surface polymerization toolkit.[19] Current strat-
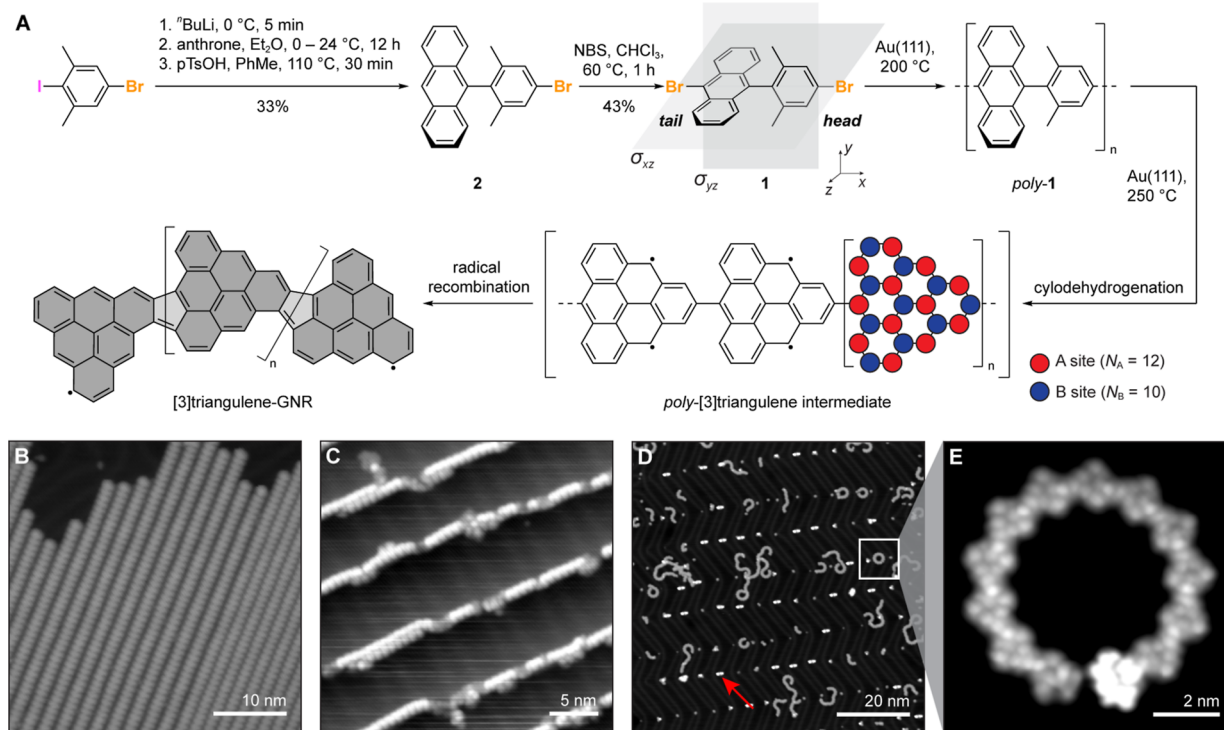
Figure 1. Synthesis and structural characterization of [3]triangulene-GNRs. (A) Schematic representation of the bottom-up synthesis of [3]triangulene-GNRs from molecular precursor **1**. (B) STM topographic image of a self-assembled island of molecular precursor **1** on Au(111) (V_s = −2.0 V, I_t = 20 pA). (C) STM topographic image of intermediate linear chains of *poly*-**1** following thermal annealing to 200 °C (V_s = −2.0 V, I_t = 30 pA). (D) STM topographic image of [3]triangulene-GNRs following annealing to 250 °C (V_s = 1.8 V, I_t = 20 pA). Red arrow: HH dimers at the elbow sites of the Au(111) herringbone reconstruction. (E) Bond-resolved STM image of the region highlighted by a square in (D) showing the [3]triangulene-GNR structure of regioregular [3]triangulene units fused by five-membered rings (V_s = 0.0 V, V_{ac} = 20 mV, and f = 533 Hz).

egies include exploiting templating effects,[20−23] modulating the composition and structure of the metal surface,[24−26] and leveraging steric hindrance in conjunction with dominant molecular absorption geometries.[3,27] While existing approaches place various constraints on precursor design, perhaps the most restrictive is that to form a regioregular structure, a molecular precursor must be symmetric with respect to a mirror plane perpendicular to the polymerization axis (the *x*-axis in Figure 1A). A synthetic tool for overcoming this requirement in forming regioregular NGs could spur the realization of designer quantum materials exhibiting new magnetic properties and topological phases of matter.[19,28]

Here, we report the design and on-surface synthesis of [3]triangulene-GNRs—regioregular [3]triangulene chains featuring fused cyclopentadiene rings. We describe a regioselective surface-catalyzed radical step-growth polymerization between phenyl- and anthracenyl-centered radicals and demonstrate that a regioregular GNR can be formed even though the molecular building block lacks a mirror plane perpendicular to the polymerization axis. The origin of this unusual selectivity is supported by ab initio calculations of the on-surface coupling mechanism. Scanning tunneling spectroscopy (STS) reveals that arranging [3]triangulene ZMs in a 1D superlattice gives rise to GNRs with a narrow band gap (E_g = 730 meV) and ZM end states. We construct an effective tight-binding (TB) model to describe the GNR electronic structure on the basis of quantum mechanical hopping of electrons between ZMs on adjacent [3]triangulene units and the topological origin of the ZM end states.

RESULTS AND DISCUSSION

Synthesis of Molecular Precursors and Surface-Assisted Growth of [3]triangulene-GNRs. The synthesis of molecular precursor **1** for [3]triangulene GNRs is depicted in Figure 1A. Chemoselective lithiation of 5-bromo-2-iodo-1,3-dimethylbenzene followed by nucleophilic addition to anthrone gave an intermediate tertiary alcohol.[9] Acid-catalyzed dehydration and rearomatization yielded **2**. Bromination of the 10-anthracenyl position in **2** using *N*-bromosuccinimide gave the molecular precursor for [3]triangulene-GNRs, 9-bromo-10-(4-bromo-2,6-dimethylphenyl)anthracene (**1**). Samples of [3]triangulene-GNRs were prepared following established surface-assisted bottom-up GNR growth protocols. Molecular precursor **1** was sublimed in ultrahigh vacuum from a Knudsen cell evaporator onto a Au(111) surface held at 25 °C. Figure 1B shows a representative topographic STM image of the self-assembled molecular arrangement of precursor **1** into linear structures (Figure S1A). Step-growth polymerization of **1** was induced by annealing the molecule-decorated surface to *T* = 200 °C. Topographic STM images show linear chains of *poly*-**1** localized exclusively along the Au(111) step edges (Figures 1C and S1B,C). A second annealing step at *T* = 250 °C induced both thermal cyclodehydrogenation and radical recombination giving rise to fully fused [3]triangulene-GNRs. Topographic STM images of annealed GNR samples show ribbons with varying degrees of curvature, ranging in length from 5 to 20 nm (Figures 1D and S1D−F). Bond-resolved STM (BRSTM) imaging with CO-functionalized tips reveals a structure of [3]triangulene units fused via five-membered rings along the backbone of the GNR (Figure 1E). The relative orientation of
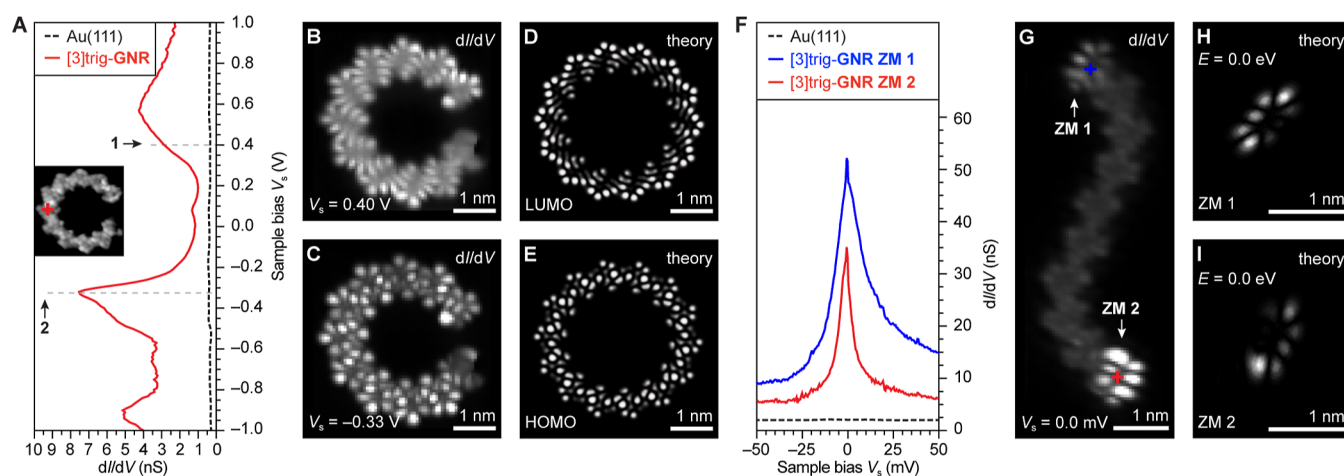
Figure 2. Electronic structure of [3]triangulene-GNRs. (A) Constant height STS dI/dV spectrum recorded on a [3]triangulene-GNR at the position marked by a red cross in the inset BRSTM image (spectroscopy: V_{ac} = 1 mV, f = 533 Hz; imaging: V_s = 0.0 V, V_{ac} = 20 mV, f = 533 Hz). (B,C) Constant height dI/dV maps recorded at the indicated biases (V_{ac} = 20 mV, f = 533 Hz). (D,E) DFT-simulated LDOS maps of the CB and VB of [3]triangulene-GNRs. A cyclic [3]triangulene-GNR 14-mer was used to reproduce the *cis* geometry of the [3]triangulene-GNR. (F) Constant height low bias dI/dV spectra of the two ZMs associated with the [3]triangulene-GNR end states recorded at the positions marked by crosses in (G) (spectroscopy: V_{ac} = 0.5 mV, f = 533 Hz; imaging: V_s = 60 mV, V_{ac} = 20 mV, and f = 533 Hz). (G) Constant height dI/dV map recorded at V_s = 0.0 mV (V_{ac} = 20 mV, and f = 533 Hz). (H,I) DFT-simulated LDOS maps (E = 0.0 eV) of the ZMs for the same [3]triangulene-GNR structure shown in (G).

each [3]triangulene building block in the GNR backbone suggests that the on-surface polymerization giving rise to *poly-1* strongly favors C−C bond formation from a head-to-tail (HT) configuration. We herein refer to the *m*-xylyl ring in **1** as the head and the anthracenyl group as the tail end of the molecule (Figure 1A). The observed HT selectivity is remarkable as coupling of the radical intermediate formed from precursor **1** should in principle lead to three discrete geometries. In addition to the observed HT coupling, we would also expect the sterically less encumbered head-to-head (HH) coupling, forming a biphenyl linkage, and tail-to-tail (TT) coupling, giving rise to a bisanthene core, to occur. Despite these alternative possible reaction pathways, the backbone of [3]triangulene-GNRs exclusively features the HT geometry. The only evidence for HH coupling is the observation of dimers localized at the elbow sites of the Au(111) herringbone reconstruction (Figure 1D). The HH reaction intermediate appears to be trapped at the dimer stage and does not react further to form extended oligomers or polymers.

BRSTM images further reveal that the five-membered ring formation between adjacent [3]triangulene units gives rise to patterns of *cis*- and *trans*-linkages that induce local curvature of the ribbon. An apparent preference for the *cis*-conformation, comprising greater than 90% of the linkages, leads to the observed spiral topology of [3]triangulene-GNRs. The proposed *poly*-[3]triangulene intermediate (Figure 1A) could not be trapped on the surface, suggesting that the activation barrier for five-membered ring formation is small. This is further supported by STM images of partially cyclodehydrogenated *poly*-**1** that show fused sections featuring the characteristic curvature induced by the *poly*-[3]triangulene backbone (Figures 1A and S1B,C). Concurrent with the initial cyclodehydrogenation of *poly*-**1**, the emergent triplet π-radical character localized on the C atoms of the majority sublattice facilitates radical recombination to form additional C−C bonds. Surface-catalyzed dehydrogenation forms the π-conjugated five-membered rings that define the [3]-triangulene-GNR backbone. This sequence bears resemblance

to recent reports of π-radical recombination and cyclo-dehydrogenation in solution-based transformations.[29−31] Despite the efficient hybridization of π-radical states of adjacent [3]triangulene units, a finite GNR retains two unpaired electrons (one at either end of the ribbon) that are expected to give rise to characteristic ZMs or localized end states.

Electronic Structure Characterization of [3]-Triangulene-GNR. After elucidating the chemical structure of [3]triangulene-GNRs, we set out to explore their local electronic structures using tunneling spectroscopy (Figures 2 and S2, S3). A representative dI/dV point spectrum recorded at the position highlighted by the red cross in the topographic STM image (Figure 2A inset) shows two prominent features: a broad shoulder at V_s = 400 mV (state 1) and a peak at V_s = −330 mV (state 2). Constant height dI/dV maps of state 1 (Figure 2B) show a diffuse striated pattern that closely matches the density functional theory (DFT)-simulated LDOS map of the LUMO for a cyclic tetradecamer, a proxy for the conduction band (CB) (Figure 2D). Similarly, dI/dV maps recorded at V_s = −330 mV (Figure 2C) show a distinctive nodal pattern that closely matches the DFT-simulated LDOS map of the corresponding HOMO, a proxy for the valence band (VB) (Figure 2E). The resulting experimental STS band gap of [3]triangulene-GNRs on Au(111) is then $E_{g,exp}$ ∼ 0.7 eV.

Differential conductance maps recorded along the center of [3]triangulene-GNRs show the typical signature of a bulk semiconductor—a vanishing density of states (DOS) at V_s = 0.0 mV (Figure 2G). Both ends of the ribbon exhibit bright nodal features generally associated with low-bias end states. dI/dV point spectra recorded over a narrow bias window (−50 mV ≤ V_s ≤ + 50 mV) at the positions highlighted by crosses in Figure 2G show sharp peaks centered at V_s = 0.0 mV. These prominent features are characteristic of Kondo resonances arising from the scattering of conduction electrons in the Au substrate by the magnetic moment of localized unpaired electron spins.[32−35] The origin of these ZMs can be traced back to five-membered ring formation along the backbone of

[3]triangulene-GNRs. Pairwise π-radical recombination leaves behind a single unpaired electron at either end of the ribbon that manifests as a $S = 1/2$ ZM end state localized on the terminating [3]triangulene unit (Figure 1A). This interpretation is further supported by DFT-simulated LDOS maps of a finite [3]triangulene-GNR sampled near the Fermi level (E_F). The characteristic nodal structure of the ZM end states in dI/dV maps is faithfully reproduced by theory at $E = 0.0$ eV (Figure 2H,I).

First-Principles Electronic Structure Calculation. We further explored the electronic structure of [3]triangulene-GNRs using ab initio DFT. Figure 3A,B shows the theoretical
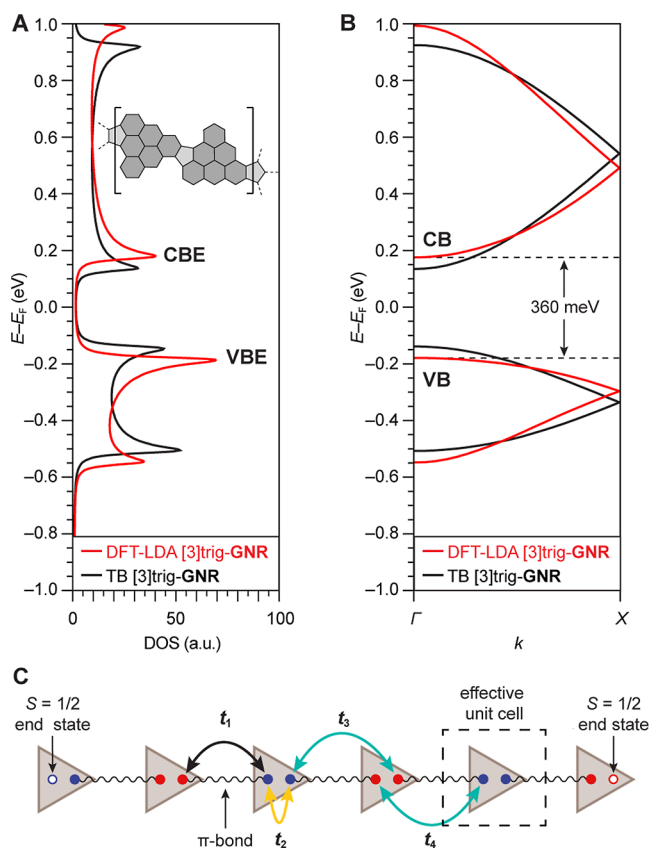
Figure 3. First-principle calculations and effective TB model of [3]triangulene-GNRs. (A) DOS of [3]triangulene-GNRs calculated from DFT-LDA (red) and an effective TB model (black) showing density increase at band edges characteristic of 1D bands. A model of the fully *trans*-linked [3]triangulene-GNR shown in the inset was used in DFT calculations. (B) Band structure of [3]triangulene-GNRs calculated from DFT-LDA (red) and an effective TB model (black). (C) Effective TB model using basis states that represent the isolated [3]triangulene ZMs coupled via nearest-neighbor electronic hopping parameters t_1 (black) and t_2 (yellow) and next-nearest-neighbor hopping parameters t_3 and t_4 (cyan). A ZM at each ribbon end that is weakly coupled to the other ZMs forms an $S = 1/2$ end state. Blue and red filled circles represent ZMs on the A and B sublattice, respectively.

DOS and band structure of [3]triangulene-GNRs calculated using the local density approximation (LDA) for the exchange—correlation potential. The VB and CB are separated by a semiconducting energy gap of $E_{g,LDA} \sim 0.36$ eV. The CB and VB are flanked by sizable energy gaps that isolate them from the CB + 1 and VB − 1 (Figure S4). DFT-LDA typically underestimates band gaps relative to experimental values since

it does not account for self-energy and image charge screening effects from the metal surface.[36−38] The band structure of [3]triangulene-GNRs was also calculated using ab initio GW calculations,[38] which apply a self-energy correction (Figure S5). A larger band gap of $E_{g,GW} \sim 1.86$ eV was determined. GW and LDA calculations define the upper and lower theoretical bounds, respectively, and bracket the experimental gap $E_{g,exp} \sim 0.7$ eV determined by STS. A model of the all-*trans* [3]triangulene-GNR was used in the calculations to ensure a periodic unit cell (Figure 3A inset). To examine the impact of linkage geometry on the calculations, the molecular orbital energies of the all-*cis* cyclic tetradecamer were calculated using DFT-LDA (Figure S6). The calculated HOMO−LUMO gap $E_{g,DFT} \sim 0.35$ eV is comparable to the LDA-calculated band gap, and thus the ab initio calculations are minimally affected by the linkage geometry.

The low-energy electronic structure of [3]triangulene-GNRs that emerges from ab initio DFT can be captured in an effective TB model (Figure 3C). Each triangulene unit bears two ZMs (with on-site energy ε_0) that form the basis states of the TB model. The recombination of two unpaired electrons to form a π-bond leads to the effective hybridization of ZMs on neighboring [3]triangulene units that is described by the hopping term t_1. This interaction leads to sublattice mixing which causes the ZMs within a [3]triangulene unit to no longer be orthogonal. The resulting intraunit interaction is denoted by the hopping term t_2. Finally, we consider next-nearest neighbor interactions summarized in the term t_{NN} which is the arithmetic mean [$t_{NN} = 1/2(t_3 + t_4)$] of the two possible next-nearest neighbor hoppings t_3 and t_4. The Hamiltonian matrix of this TB model can be expressed as

$$\mathbf{H} = \begin{pmatrix} \varepsilon_0 + 2t_{NN}\cos ka & t_2 + t_1 e^{ika} \\ t_2 + t_1 e^{-ika} & \varepsilon_0 + 2t_{NN}\cos ka \end{pmatrix}$$

$$= (\varepsilon_0 + 2t_{NN}\cos ka)\mathbf{I} + \mathbf{H}_{SSH}$$

where k is the electron momentum, a is the lattice constant, and $\mathbf{H}_{SSH}$ the standard Hamiltonian of the form of the Su−Schrieffer−Heeger (SSH) model.[3,4,39] The eigenvalues of this Hamiltonian are

$$E = \varepsilon_0 + 2t_{NN}\cos ka \pm \sqrt{t_1^2 + t_2^2 + 2t_1 t_2 \cos ka}$$

$$= \varepsilon_0 + 2t_{NN}\cos ka \pm E(k)_{SSH}$$

where the positive and negative solutions describe the CB and VB, respectively. This result is identical to the SSH model except for the next-nearest neighbor interaction term, which adds a cosinusoidal modulation to the VB and CB that breaks electron−hole symmetry and accounts for the observed asymmetry between the VB and CB in the band structure (Figure 3A,B). Optimization of the parameters ($\varepsilon_0 = -3.77$ eV, $t_1 = -428$ meV, $t_2 = 106$ meV, $t_{NN} = -145$ meV) provides a good match with the DFT band structure (see Figure S7 for the unfolded band structure).

Provided that $|t_{NN}| < \|t_1| - |t_2\|$, the cosine term does not induce a crossing between the VB and CB, and the [3]triangulene-GNR features the same topological properties as the SSH model. When the unit cell is centered on a π-bond between [3]triangulene units, the intracell coupling is defined by t_1 and the intercell coupling by t_2. Thus, the intracell coupling is larger than the intercell coupling, and the
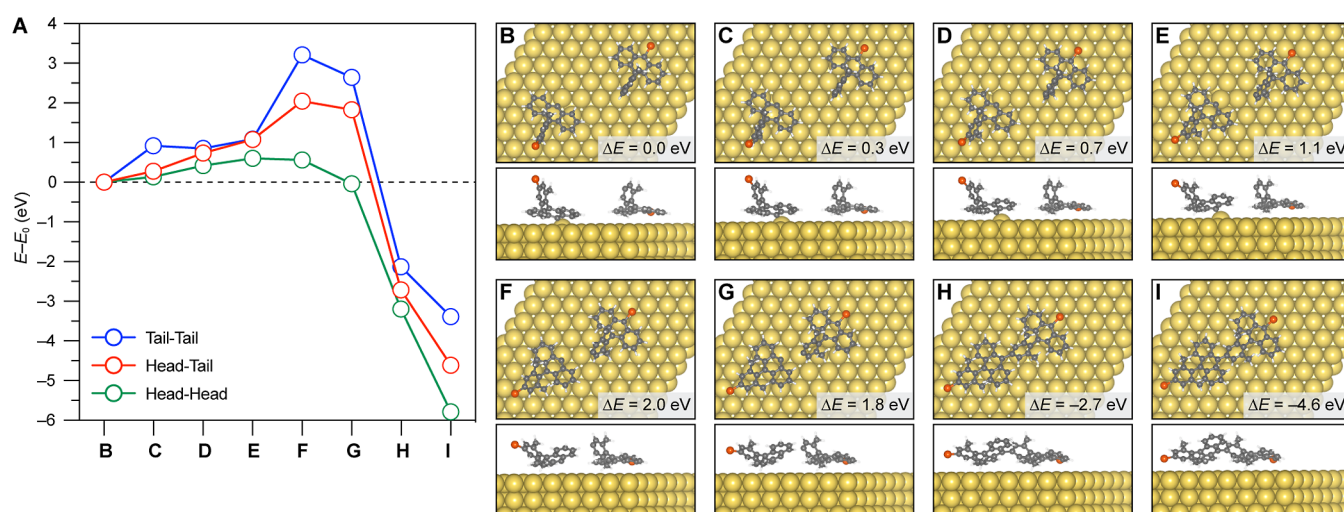
Figure 4. Mechanistic calculations of the regioselective coupling of molecular precursor **1** on Au(111). (A) Calculated reaction coordinate diagram showing TS energies corresponding to the HT, HH, and TT coupling geometries. (B) Minimized geometries of molecular precursor **1**, (C−H) intermediates, and (I) the product dimer along the HT coupling pathway.

[3]triangulene-GNR is topologically trivial. However, when the unit cell is centered on a [3]triangulene, then the intracell hopping is defined by t_2 and the intercell by t_1. Thus, intercell coupling dominates, and the [3]triangulene-GNR is topologically nontrivial. The GNR explored in Figure 2F,G is terminated by [3]triangulenes units, and the ZMs observed at either end of the ribbon correspond to the topological boundary states predicted by theory.

Computational Model for the HT Selective On-Surface Polymerization. Having resolved the electronic structure of [3]triangulene-GNRs, we return our attention to the unusual HT regioselectivity observed in the surface-assisted radical step-growth polymerization of **1**. In an effort to gain insights into the underlying mechanism that gives rise to this curious selectivity, we performed ab initio modeling using the all-electron FHI-aims code.[40] We calculated the activation barriers for the three possible C−C bond formation geometries on a Au(111) surface using DFT at the PBE + vdW + ZORA level (Figure 4A).[40−42] All three modeled reactions are exothermic, ranging between $\Delta E = -3.4$ to -5.8 eV. The highest transition state (TS) energy is predicted for the sterically challenging TT coupling ($E_a = 3.2$ eV), followed by HT ($E_a = 2.0$ eV) and HH ($E_a = 0.6$ eV) coupling. Activation barriers were determined by calculating the energies of relaxed molecular structures along the reaction sequence. The optimized adsorption geometries for the HT coupling pathway are depicted in Figure 4B−I (see Figures S6 and 7 for the TT and HH coupling pathways). Notably, anthracenyl radical intermediates formed in the thermally induced homolytic cleavage of the C−Br bonds in molecular precursor **1** are stabilized by a covalent interaction with a single Au atom protruding ∼0.8−1.0 Å from the plane of the Au(111) surface. The gradual buildup of strain in the coordination of the Au-atom, culminating in Au−C bond breakage in the TS, provides a major contribution to the activation barrier of the HT and TT reaction profile. While the former mechanism only involves the dissociation of a single Au−C bond in the TS, the latter requires the dissociation of two Au−C bonds to form the TT dimer, and accordingly its activation energy is ∼1.2 eV higher (Figure S8). Curiously, the calculated activation barrier for the formation of the HH dimer from a pair of phenyl radicals

derived from **1** is small and should in principle compete with the HT polymerization (Figure S9).

While the calculated activation barriers qualitatively reproduce the experimental selectivity for the HT over the TT coupling, the absence of HH coupling along the backbone or the ends of [3]triangulene-GNRs requires some additional discussion. A hint can be found in the presence of dimers featuring the HH bonding geometry that adsorb preferentially at the elbow sites of the Au(111) herringbone reconstruction (Figure 1D). Figure S10 shows the relaxed adsorption geometry of the corresponding intermediate at the gold surface. Anthracenyl radicals at either end of the molecule are coordinated to Au atoms of the Au(111) surface. This divalent coordination may represent a kinetic trap that precludes the participation of the HH dimer intermediate in further chain growth before the temperature reaches the threshold of desorption. The annealing of molecule-decorated surfaces to $T = 250$ °C induces a significant decrease in coverage suggesting that small-molecule HH dimers may desorb from the surface before cyclodehydrogenation of [3]triangulene-GNRs is complete. In addition to our hypotheses informed from our mechanistic calculations, a variety of other factors that may influence the observed reaction selectivity are addressed in Supporting Information Discussion 1.

■ CONCLUSIONS

We have demonstrated rational band engineering using the ZMs of [3]triangulenes assembled vertex-to-edge in a regioregular superlattice. Five-membered ring formation along the GNR backbone facilitates hybridization between ZMs that gives rise to a narrow band gap ($E_{g,exp} \sim 0.7$ eV) on a Au surface and topological boundary states akin to those described by the SSH model. The chemical bonding, band structure, and ZM end states of [3]triangulene-GNRs are fully characterized with atomic resolution using STM. TB and first-principles DFT-LDA calculations support our experimental observations. Our on-surface synthetic strategy shows that a regioregular GNR can be formed even though the molecular precursor does not feature a mirror plane perpendicular to the polymerization axis. Our results provide a framework for the deterministic design of GNR electronic structure using ZMs

and offer a new strategy for selective on-surface polymerization.

ASSOCIATED CONTENT

Supporting Information

The Supporting Information is available free of charge at https://pubs.acs.org/doi/10.1021/jacs.4c02386.

Materials and methods, synthetic procedures, STM topographic and BRSTM images, dI/dV maps, STS data, and NMR spectra (PDF)

AUTHOR INFORMATION

Corresponding Authors

Angel Rubio − *Nano-Bio Spectroscopy Group and ETSF, Universidad del País Vasco UPV/EHU, Donostia E20018, Spain; Max Planck Institute for the Structure and Dynamics of Matter, Hamburg 22761, Germany; Center for Computational Quantum Physics (CCQ), The Flatiron Institute, New York, New York 10010, United States;* orcid.org/0000-0003-2060-3151; Email: angel.rubio@mpsd.mpg.de

Steven G. Louie − *Department of Physics, University of California, Berkeley, California 94720, United States; Materials Sciences Division, Lawrence Berkeley National Laboratory, Berkeley, California 94720, United States;* orcid.org/0000-0003-0622-0170; Email: sglouie@berkeley.edu

Michael F. Crommie − *Department of Physics, University of California, Berkeley, California 94720, United States; Materials Sciences Division, Lawrence Berkeley National Laboratory, Berkeley, California 94720, United States; Kavli Energy NanoSciences Institute at the University of California Berkeley and the Lawrence Berkeley National Laboratory, Berkeley, California 94720, United States;* orcid.org/0000-0001-8246-3444; Email: crommie@berkeley.edu

Felix R. Fischer − *Department of Chemistry, University of California, Berkeley, California 94720, United States; Materials Sciences Division, Lawrence Berkeley National Laboratory, Berkeley, California 94720, United States; Kavli Energy NanoSciences Institute at the University of California Berkeley and the Lawrence Berkeley National Laboratory, Berkeley, California 94720, United States; Bakar Institute of Digital Materials for the Planet, Division of Computing, Data Science, and Society, University of California, Berkeley, California 94720, United States;* orcid.org/0000-0003-4723-3111; Email: ffischer@berkeley.edu

Authors

Michael C. Daugherty − *Department of Chemistry, University of California, Berkeley, California 94720, United States;* orcid.org/0000-0002-3348-561X

Peter H. Jacobse − *Department of Physics, University of California, Berkeley, California 94720, United States;* orcid.org/0000-0002-0777-6050

Jingwei Jiang − *Department of Physics, University of California, Berkeley, California 94720, United States; Materials Sciences Division, Lawrence Berkeley National Laboratory, Berkeley, California 94720, United States;* orcid.org/0000-0002-0949-4401

Joaquim Jornet-Somoza − *Nano-Bio Spectroscopy Group and ETSF, Universidad del País Vasco UPV/EHU, Donostia E20018, Spain; Max Planck Institute for the Structure and*

Dynamics of Matter, Hamburg 22761, Germany; orcid.org/0000-0002-6721-1393

Reis Dorit − *Department of Chemistry, University of California, Berkeley, California 94720, United States*

Ziyi Wang − *Department of Chemistry, University of California, Berkeley, California 94720, United States; Materials Sciences Division, Lawrence Berkeley National Laboratory, Berkeley, California 94720, United States; Kavli Energy NanoSciences Institute at the University of California Berkeley and the Lawrence Berkeley National Laboratory, Berkeley, California 94720, United States;* orcid.org/0000-0003-1049-5038

Jiaming Lu − *Department of Physics, University of California, Berkeley, California 94720, United States*

Ryan McCurdy − *Department of Chemistry, University of California, Berkeley, California 94720, United States;* orcid.org/0000-0001-7319-4836

Weichen Tang − *Department of Physics, University of California, Berkeley, California 94720, United States; Materials Sciences Division, Lawrence Berkeley National Laboratory, Berkeley, California 94720, United States;* orcid.org/0000-0002-1945-5369

Complete contact information is available at:
https://pubs.acs.org/10.1021/jacs.4c02386

Author Contributions

M.C.D., P.H.J., and J.J. contributed equally. All authors have given approval to the final version of the manuscript.

Notes

The authors declare no competing financial interest.

ACKNOWLEDGMENTS

■ REFERENCES

(1) Moore, G. E. Cramming more components onto integrated circuits. *Proc. IEEE* **1998**, *86*, 82−85.

(2) Saraswat, V.; Jacobberger, R. M.; Arnold, M. S. Materials Science Challenges to Graphene Nanoribbon Electronics. *ACS Nano* **2021**, *15*, 3674−3708.

(3) Rizzo, D. J.; Veber, G.; Cao, T.; Bronner, C.; Chen, T.; Zhao, F. Z.; Rodriguez, H.; Louie, S. G.; Crommie, M. F.; Fischer, F. R. Topological band engineering of graphene nanoribbons. *Nature* **2018**, *560*, 204−208.

(4) Groning, O.; Wang, S. Y.; Yao, X. L.; Pignedoli, C. A.; Borin Barin, G.; Daniels, C.; Cupo, A.; Meunier, V.; Feng, X. L.; Narita, A.; Müllen, K.; Ruffieux, P.; Fasel, R. Engineering of robust topological quantum phases in graphene nanoribbons. *Nature* **2018**, *560*, 209−213.

(5) Rizzo, D. J.; Veber, G.; Jiang, J.; McCurdy, R.; Cao, T.; Bronner, C.; Chen, T.; Louie, S. G.; Fischer, F. R.; Crommie, M. F. Inducing metallicity in graphene nanoribbons via zero-mode superlattices. *Science* **2020**, *369*, 1597−1603.

(6) McCurdy, R. D.; Delgado, A.; Jiang, J. W.; Zhu, J. M.; Wen, E. C. H.; Blackwell, R. E.; Veber, G. C.; Wang, S. K.; Louie, S. G.; Fischer, F. R. Engineering Robust Metallic Zero-Mode States in Olympicene Graphene Nanoribbons. *J. Am. Chem. Soc.* **2023**, *145*, 15162−15170.

(7) Cao, T.; Zhao, F. Z.; Louie, S. G. Topological Phases in Graphene Nanoribbons: Junction States, Spin Centers, and Quantum Spin Chains. *Phys. Rev. Lett.* **2017**, *119*, 076401.

(8) de Oteyza, D. G.; Frederiksen, T. Carbon-based nanostructures as a versatile platform for tunable π-magnetism. *J. Phys. Condens. Matter* **2022**, *34*, 443001.

(9) Yazyev, O. V. Emergence of magnetism in graphene materials and nanostructures. *Rep. Prog. Phys.* **2010**, *73*, 056501.

(10) Wang, W. L.; Yazyev, O. V.; Meng, S.; Kaxiras, E. Topological Frustration in Graphene Nanoflakes: Magnetic Order and Spin Logic Devices. *Phys. Rev. Lett.* **2009**, *102*, 157201.

(11) Morita, Y.; Suzuki, S.; Sato, K.; Takui, T. Synthetic organic spin chemistry for structurally well-defined open-shell graphene fragments. *Nat. Chem.* **2011**, *3*, 197−204.

(12) Pavlicek, N.; Mistry, A.; Majzik, Z.; Moll, N.; Meyer, G.; Fox, D. J.; Gross, L. Synthesis and characterization of triangulene. *Nat. Nanotechnol.* **2017**, *12*, 308−311.

(13) Mishra, S.; Beyer, D.; Eimre, K.; Liu, J. Z.; Berger, R.; Groning, O.; Pignedoli, C. A.; Müllen, K.; Fasel, R.; Feng, X. L.; Ruffieux, P. Synthesis and Characterization of π-Extended Triangulene. *J. Am. Chem. Soc.* **2019**, *141*, 10621−10625.

(14) Su, J.; Telychko, M.; Hu, P.; Macam, G.; Mutombo, P.; Zhang, H. J.; Bao, Y.; Cheng, F.; Huang, Z. Q.; Qiu, Z. Z.; Tan, S. J. R.; Lin, H.; Jelinek, P.; Chuang, F. C.; Wu, J. S.; Lu, J. Atomically precise bottom-up synthesis of π-extended [5]triangulene. *Sci. Adv.* **2019**, *5*, No. eaav7717.

(15) Mishra, S.; Xu, K.; Eimre, K.; Komber, H.; Ma, J.; Pignedoli, C. A.; Fasel, R.; Feng, X. L.; Ruffieux, P. Synthesis and characterization of [7]triangulene. *Nanoscale* **2021**, *13*, 1624−1628.

(16) Mishra, S.; Beyer, D.; Eimre, K.; Ortiz, R.; Fernandez-Rossier, J.; Berger, R.; Gröning, O.; Pignedoli, C. A.; Fasel, R.; Feng, X. L.; Ruffieux, P. Collective All-Carbon Magnetism in Triangulene Dimers. *Angew. Chem., Int. Ed.* **2020**, *59*, 12041−12047.

(17) Cheng, S. Q.; Xue, Z. J.; Li, C.; Liu, Y. F.; Xiang, L. J.; Ke, Y. Q.; Yan, K.; Wang, S. Y.; Yu, P. On-surface synthesis of triangulene trimers via dehydration reaction. *Nat. Commun.* **2022**, *13*, 1705.

(18) Mishra, S.; Catarina, G.; Wu, F. P.; Ortiz, R.; Jacob, D.; Eimre, K.; Ma, J.; Pignedoli, C. A.; Feng, X. L.; Ruffieux, P.; Fernandez-Rossier, J.; Fasel, R. Observation of fractional edge excitations in nanographene spin chains. *Nature* **2021**, *598*, 287−292.

(19) Clair, S.; de Oteyza, D. G. Controlling a Chemical Coupling Reaction on a Surface: Tools and Strategies for On-Surface Synthesis. *Chem. Rev.* **2019**, *119*, 4717−4776.

(20) Lin, T.; Shang, X. S.; Adisoejoso, J.; Liu, P. N.; Lin, N. Steering On-Surface Polymerization with Metal-Directed Template. *J. Am. Chem. Soc.* **2013**, *135*, 3576−3582.

(21) Li, D. Y.; Zhu, Y. C.; Li, S. W.; Shu, C. H.; Liu, P. N. Post-Functionalization of Supramolecular Polymers on Surface and the Chiral Assembly-Induced Enantioselective Reaction. *Angew. Chem., Int. Ed.* **2021**, *60*, 11370−11377.

(22) Zhang, R.; Lyu, G. Q.; Li, D. Y.; Liu, P. N.; Lin, N. A. Template-controlled Sonogashira cross-coupling reactions on a Au(111) surface. *Chem. Commun.* **2017**, *53*, 1731−1734.

(23) Xing, S. P.; Zhang, Z.; Fei, X. Y.; Zhao, W.; Zhang, R.; Lin, T.; Zhao, D. L.; Ju, H. X.; Xu, H.; Fan, J.; Zhu, J. F.; Ma, Y. Q.; Shi, Z. L. Selective on-surface covalent coupling based on metal-organic coordination template. *Nat. Commun.* **2019**, *10*, 70.

(24) Schulz, F.; Jacobse, P. H.; Canova, F. F.; van der Lit, J.; Gao, D. Z.; van den Hoogenband, A.; Han, P.; Klein Gebbink, R. J.; Moret, M. E.; Joensuu, P. M.; Swart, I.; Liljeroth, P. Precursor Geometry Determines the Growth Mechanism in Graphene Nanoribbons. *J. Phys. Chem. C* **2017**, *121*, 2896−2904.

(25) Fan, Q. T.; Dai, J. Y.; Wang, T.; Kuttner, J.; Hilt, G.; Gottfried, J. M.; Zhu, J. F. Confined Synthesis of Organometallic Chains and Macrocycles by Cu-O Surface Templating. *ACS Nano* **2016**, *10*, 3747−3754.

(26) Wang, S. Y.; Sun, Q.; Gröning, O.; Widmer, R.; Pignedoli, C. A.; Cai, L. L.; Yu, X.; Yuan, B. K.; Li, C.; Ju, H. X.; Zhu, J. F.; Ruffieux, P.; Fasel, R.; Xu, W. On-surface synthesis and characterization of individual polyacetylene chains. *Nat. Chem.* **2019**, *11*, 924−930.

(27) Wang, S.; Nishiuchi, T.; Pignedoli, C. A.; Yao, X. L.; Di Giovannantonio, M.; Zhao, Y.; Narita, A.; Feng, X.; Müllen, K.; Ruffieux, P.; et al. Steering on-surface reactions through molecular steric hindrance and molecule-substrate van der Waals interactions. *Quantum Front.* **2022**, *1*, 23.

(28) Wang, H. M.; Wang, H. S.; Ma, C. X.; Chen, L. X.; Jiang, C. X.; Chen, C.; Xie, X. M.; Li, A. P.; Wang, X. R. Graphene nanoribbons for quantum electronics. *Nat. Rev. Phys.* **2021**, *3*, 791−802.

(29) Jiao, T. Y.; Ni, Y.; Xu, T. T.; Hou, X. D.; Wu, S. F.; Ren, L. B.; Gu, Y. W.; Miao, X. H.; Sun, Z.; Wu, J. S. Synthesis of monolayer and persistent bilayer graphene fragments by using a radical-mediated coupling approach. *Nat. Synth.* **2023**, *2*, 1104−1115.

(30) Shen, T.; Zou, Y.; Hou, X. D.; Wei, H. P.; Ren, L. B.; Jiao, L. Y.; Wu, J. S. Bis-peri-dinaphtho-rylenes: Facile Synthesis via Radical-Mediated Coupling Reactions and their Distinctive Electronic Structures. *Angew. Chem., Int. Ed.* **2023**, *62*, No. e202311928.

(31) Bernhardt, A.; Cavlovic, D.; Mayländer, M.; Blacque, O.; Cruz, C. M.; Richert, S.; Juríček, M. π-Radical Cascade to a Chiral Saddle-Shaped Peropyrene. *Angew. Chem., Int. Ed.* **2024**, *63*, No. e202318254.

(32) Madhavan, V.; Chen, W.; Jamneala, T.; Crommie, M. F.; Wingreen, N. S. Tunneling into a single magnetic atom: Spectroscopic evidence of the Kondo resonance. *Science* **1998**, *280*, 567−569.

(33) Ternes, M.; Heinrich, A. J.; Schneider, W. D. Spectroscopic manifestations of the Kondo effect on single adatoms. *J. Phys. Condens. Matter* **2009**, *21*, 053001.

(34) Li, J. C.; Sanz, S.; Corso, M.; Choi, D. J.; Pena, D.; Frederiksen, T.; Pascual, J. I. Single spin localization and manipulation in graphene open-shell nanostructures. *Nat. Commun.* **2019**, *10*, 200.

(35) Wen, E. C. H.; Jacobse, P. H.; Jiang, J.; Wang, Z. Y.; McCurdy, R. D.; Louie, S. G.; Crommie, M. F.; Fischer, F. R. Magnetic Interactions in Substitutional Core-Doped Graphene Nanoribbons. *J. Am. Chem. Soc.* **2022**, *144*, 13696−13703.

(36) Thygesen, K. S.; Rubio, A. Renormalization of Molecular Quasiparticle Levels at Metal-Molecule Interfaces: Trends across Binding Regimes. *Phys. Rev. Lett.* **2009**, *102*, 046802.

(37) Neaton, J. B.; Hybertsen, M. S.; Louie, S. G. Renormalization of molecular electronic levels at metal-molecule interfaces. *Phys. Rev. Lett.* **2006**, *97*, 216405.

(38) Hybertsen, M. S.; Louie, S. G. Electron Correlation in Semiconductors and Insulators - Band-Gaps and Quasi-Particle Energies. *Phys. Rev. B: Condens. Matter Mater. Phys.* **1986**, *34*, 5390−5413.

(39) Su, W. P.; Schrieffer, J. R.; Heeger, A. J. Solitons in Polyacetylene. *Phys. Rev. Lett.* **1979**, *42*, 1698−1701.

(40) Blum, V.; Gehrke, R.; Hanke, F.; Havu, P.; Havu, V.; Ren, X. G.; Reuter, K.; Scheffler, M. Ab initio molecular simulations with numeric atom-centered orbitals. *Comput. Phys. Commun.* **2009**, *180*, 2175−2196.

(41) Perdew, J. P.; Burke, K.; Ernzerhof, M. Generalized gradient approximation made simple. *Phys. Rev. Lett.* **1996**, *77*, 3865−3868.

(42) Tkatchenko, A.; Scheffler, M. Accurate Molecular Van der Waals Interactions from Ground-State Electron Density and Free-Atom Reference Data. *Phys. Rev. Lett.* **2009**, *102*, 073005.